Importance of Windscreen Modelling Approach for Head Injury Prediction.

Victor S. Alvarez, Svein Kleiven

Abstract The objective of this study is to evaluate the capability of two modelling approaches in capturing both accelerations and deformations from head impacts, and to evaluate the effect of modelling approach on brain injury prediction. The first approach is a so-called smeared technique, in which the properties of the two glass sheets and the intermediate polyvinyl butyral (PVB) are combined and divided into two coinciding shell layers, of which one can fracture. The second approach consists of three shell layers, representing the glass and PVB, separated by the distance of their thickness, using a non-local failure criterion to initiate fracture in the glass. The two modelling approaches are compared to impact experiments of flat circular windscreens, measuring deformations and accelerations as well as accelerations from impacts against full vehicle windscreens. They are also used to study head-to-windscreen impacts using a detailed Finite Element (FE) model, varying velocity, impact direction and impact point. Only the non-local failure model is able to adequately capture both the accelerations and deformations of an impactor. The FE head model simulations also reveal that the choice of modelling approach has a large effect on the both localisation of the strain in the brain and the characteristics of the strain-time curve, with a difference in peak strain between 8% and 40%.

Keywords Windscreen modelling, Finite Element Method (FEM), Brain injury, Pedestrian, Head impact.

I. INTRODUCTION

Pedestrians and bicyclists involved in vehicle accidents constitute up to 54% of all fatalities caused by traffic accidents [1]. German in-depth investigation data (GIDAS) show that up to 60% of all pedestrians sustain a head injury, of which 19.8% are caused by the windscreen pane [2]. According to [3] the most frequent impact point for the head is the lower part of the windscreen area, with a large variation of head injury types, with impacts near the windscreen frame leading to higher severity injuries. In [4] it is reported that 26% of the severe head injuries in the GIDAS database from 1999 to 2008 derived from an impact to the windscreen area. Of the pure glass impacts, 73% were brain injuries. The probability of impacting the windscreen area also increases with higher collision speeds, with a probability of 60.4% between 51 km/h to 60 km/h [2].

To better understand head injury mechanisms and develop safer vehicles, computational models are being used to an increasing extent. It is clear that there are many parameters that can affect the outcome of an impact to the head, where accelerations determine the magnitude of the impact. But as the brain is sensitive to rotational motion due to its low shear modulus [5–7], it is also important to capture the motion of the head correctly. This emphasises the importance to model all boundary conditions to the head in as detailed a manner as possible and also the need for a windscreen model that can capture both accelerations and deformations correctly.

Most vehicle windscreens are constructed in a similar way with two layers of glass and a thin interlayer of polyvinyl butyral (PVB), so-called laminated glass, which aims to prevent fragments of glass flying away when fractured. The glass is bonded to the PVB and when the glass fails, the fragments are held in place by the PVB layer. As a result of this composite structure, the laminated glass attains a relatively complex pattern of failure that can be divided into the five phases described in [8], where the behaviour is initially elastic and, as the two glass layers fail, the response becomes non-linear. A variety of approaches have been employed to capture this behaviour in Finite Element (FE) models for dynamic explicit solvers, from detailed 3D solid elements representing each layer, both in blast [9][10] and impact applications [11][12], to a combination of shell elements and solid elements [13]. A commonly used approach in impact applications is the so-called

V. S. Alvarez (e-mail: vicsa@kth.se; tel: +4687904876,) is a PhD student in Biomechanics of Head and Neck Injuries and S. Kleiven is Prof. at Neuronics Engineering, both at the School of Technology and Health, KTH - Royal Institute of Technology, Sweden.

smeared technique using two superimposed shell elements combining the pre- and post-failure behaviour where one of the shell layers can be deleted with failure [8][14][15]. Different groups have also used different approaches to model the failure of glass, from simple maximum Von Mises stress or maximum principal strain, to more complex, constitutive failure models. There is also a laminated glass model available in LS-Dyna that takes into account the combination of two materials. In [16] a failure model based on experimental observations is introduced, namely that the laminated glass does not fail directly after impact by assuming that a critical energy value has to be exceeded within a finite region before failure. In the study they also performed well controlled experiments with both planar and curved laminated glass specimens, measuring accelerations and deformations where they could show a good agreement for their model with the experiments performed. This model has since been included in the LS-Dyna *MAT_ADD_EROSION, where the two parameters developed in the study can be included and failure initiation is based on a principal stress limit value.

A benefit of using solid elements is the possibility of introducing advanced material models and detailed geometrical description. On the other hand, the degrees of freedom (DoF) and number of nodes quickly increase as the element size should be in the same order as the thickness of the thin PVB interlayer, and can thus give very long calculation times. It has also been suggested that there is no major benefit in using 3D elements [16]. For implementation in pedestrian impact situations, the use of shell elements is preferable since the calculation times are already large due to the rest of the models in such simulations.

This study aims to compare two different modelling approaches used in vehicle impact simulations in order to gain a deeper understanding of their effect on brain injury prediction. The objective is to compare their performance to the experiments in [16] and investigate the influence of the models on strains in the brain by impacting a detailed FE head model on the windscreen models at relevant points based on real-world data.

II. METHODS

Two FE models of windscreen glass were developed: one based on the smeared technique; and one based on the non-local failure model [16]. Based on the experiments in [16], two meshes were created with each model: one circular plate; and one of a full vehicle windscreen from a common passenger car. The two meshes were given the same approximate element size of 20 mm based on a mesh convergence study showing small effects of further mesh refinement, presented in Appendix A. Based on the technique for creating the models the material properties were adjusted for each model. Both models were tested for their performance, comparing with both deformation and acceleration data from [16]. All simulations were performed using LS-Dyna (revision 8.0.0), and all accelerations from the simulations were filtered with SAE 1000.

Material Properties

Glass has linear elastic behaviour with a Young's modulus of 70 GPa [8][13–16] and Poisson's ratio of 0.23 [8][13]. It exhibits brittle fracture and has slightly varying failure values for both ultimate stress and strain. In this study the values from [16] of 60 MPa was used for the non-local failure model, and for the smeared model 50 MPa with plastic strain limit of 0.001 from [15]. The two different ultimate stress values were used since they were chosen empirically in each study for the respective model.

PVB exhibits nonlinear deformation behaviour that can be described with a hyperplastic model like Mooney-Rivlin [13][18] or an Ogden Rubber [18][19]. It also exhibits viscoelastic effects, considered with a linear viscoelastic model in [21] or with a nonlinear viscoelastic model in [8][15]. However, it has been shown that there is little difference in models with and without viscoelasticity [20], which was also confirmed when performing preliminary simulations of the experiments in [16], and it was therefore omitted in this study. The failure of PVB is also ignored as reported failure strain values of 200% [8] are expected to lie well beyond the strains experienced in impacts scenarios simulated in this study.

Smeared Model

The smeared model presented in [14] is based on two coinciding shell element layers with the same thickness: one representing a combination of the two glass layers and the PVB before fracture; the other a combination of fractured and non-fractured glass and the PVB. The stiffness before fracture is adjusted by introducing an equivalent thickness t_E given by:

$$t_E = \sqrt[3]{t_G^3 + 3t_G(t_G + t_{PVB})^2 + \frac{E_{PVP}}{2E_G} t_{PVB}^3}, \quad (1)$$

where t_G and t_{PVB} are the thicknesses of the glass and PVB layer, respectively, and E_G and E_{PVB} are the Young's moduli for the glass and PVB, respectively. Due to this change, the density has to be adjusted to maintain the total mass using:

$$\rho_E = \frac{\rho_G t_G + \frac{1}{2}\rho_{PVB} t_{PVB}}{t_E}. \quad (2)$$

After failure it is assumed that the glass layer on the tensile side loses all its stiffness, but that the glass on the compressive side remains intact. To represent this, the elements in one of the two layers are deleted when reaching a given stress value, while the elements in the non-failure layer are assigned the Young's modulus for the state after fracture given by:

$$E^{II} = \frac{1}{t_G^3}\left[E_G\left(t_G^3 + 3t_G t_{PVB}^2\right) + E_{PVB}(t_{PVB}^3 + 3t_{PVB} t_G^2)\right]. \quad (3)$$

The shell elements of the failure layer are given a Young' modulus that maintains the correct bending stiffness before fracture, given by:

$$E_{G,mod} = 2E_G - E^{II}. \quad (4)$$

This model was implemented for impact in [15] using linear elastic material properties for both glass and PVB, with failure controlled by plastic strain and a tied penalty based contact between the two coinciding shell layers. Experiments were conducted with a standard EEVC adult head form with a weight of 4.8 kg to test the model. The simulated accelerations in their study only seem to agree marginally, having similar magnitudes of the peak values as the experiments. The material properties presented in [15] were used to calculate the smeared properties based on the glass and PVB thickness from [16] (see Appendix B).

Non-local Failure Model

A three-shell layered model was constructed to incorporate the failure model introduced in [16]. The meshes of the three layers were identical, but given an offset equal to half the shell thicknesses, tied with a penalty based contact. Each shell layer was given the thickness equal to the actual thickness of the three layers in [16], see Fig. 1.

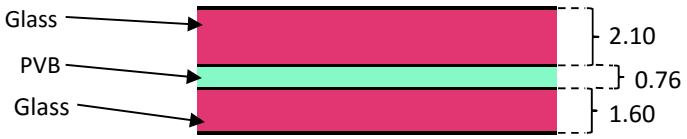

Fig. 1. Cross-section and thickness of plies (mm) of windscreen glass used in [16].

The non-local failure model is implemented for the glass plies, with failure initiation in the elements when the strain energy reaches a critical value E_c within a finite region given by the radius R_c,, as defined in [16], calculated at each time step. In LS-Dyna this is implemented together with a principal stress failure criterion. When the principal stress in an element reaches the critical value, the corresponding element is flagged as the centre of impact. Thereafter, the internal energy inside the region R_c around the centre of impact is tested against the product of the given critical energy E_c and a so-called *area factor,* defined as

$$Area\ Factor = \frac{total\ area\ of\ shell\ elements\ found\ inside\ circle}{2\pi \times R_c^2} \quad (5)$$

If this product is exceeded, all elements in the part are allowed to be deleted if they fulfil the critical value for the principal stress [22].

The glass layers were modelled with a linear elastic material and the non-local failure model described above. The PVB layer was modelled with *MAT_SIMPLIFIED_RUBBER/FOAM using a stress strain curve from [23] for a strain rate of 60 s^{-1}. All the material properties can be found in Appendix B.

Model performance

One set of experiments in [16] consisted of propelling head impactors of 3.5 kg, 4.8 kg and 6.3 kg in varying speeds against flat plates of laminated glass, with a thickness according to Fig. 1, fixed inside a rigid frame with a circular hole with a radius of 500 mm. A three-axis accelerometer was used to measure the accelerations from the centre of the impactors, and a set of ten laser extensometer to measure the deformations, placed uniformly (50 mm apart) from the centre to the edge. In a second set of experiments, the 4.8 kg head impactor was propelled against a windscreen from both outside and inside the windscreen, measuring the accelerations.

From the first set of experiments, results from three combinations of weight and velocity were published, seen in TABLE I, and used in the current study together with the full windscreen experiments to test the models. A validated model of the 4.8 kg NCAP impactor [24] was used in the simulations of the experiments. To create the different masses, the density of the outer foam was scaled appropriately. The boundary conditions of the plate were simplified to rigid constraint in all DoF on all edge nodes.

TABLE I
Experiments from [16] **simulated in current study**

Head Impactor	Circular plate	Windscreen	
		Outside	Inside
3.5 kg	5 m/s		
4.8 kg	10 m/s	10 m/s	10 m/s
6.3 kg	12 m/s		

Head Injury Simulations

To investigate the influence of the two different models on brain injury prediction using a FE head model, a set of windscreen impacts was simulated based on injury risk. The head was impacted at 40 km/h and 60 km/h at the centre of the windscreen and close to the A-pillar (edge). In all four cases the face was either towards the windscreen (termed front impact), or with the head rotated 90 degrees to impact the side of the head (termed side impact). Dimensions of the windscreen, head relative position and impact angle can be seen in Appendix C.

FE-head model

The head model used in this study includes the scalp, the skull, the brain, the meninges, the cerebrospinal fluid (CSF) and 11 pairs of the largest parasagittal bridging veins, with material properties adapted from [25]. The head model has been validated against several localised brain motion, intracerebral acceleration and intracranial pressure experiments [25][26]. A more detailed description and material properties can be found in Appendix D. The maximal principal Green-Lagrange strain was chosen as a predictor of CNS (Central Nervous System) injuries since it has been shown to correlate with diffuse axonal injuries [28–31], as well as for mechanical injury to the blood-brain barrier [32].

III. RESULTS

Circular Plate Impact

Fig. 2 shows the accelerations from the NCAP impactors and deformations at the centre of the plate for all sizes of impactor and impact speeds. The time of initial contact is defined as time zero. The results from [16] are compared to both the smeared model and the non-local failure model. In the first row, the results using 3.5 kg and 5 m/s impactor are presented, showing that both the smeared model and the non-local failure model give both acceleration and deformation in the same order of magnitude and shape as the experiment. At this impactor velocity the glass never fails, which is also predicted with both models. When the size and speed is

increased (the two bottom rows in Fig. 2), the glass fails in both cases. As can be seen, the smeared model highly over-predicts the acceleration (40% error) and under-predicts the deformation, and the error is larger for the higher velocity and size. The non-local failure model predicts the initial peak acceleration with an error of 6% for the 4.8 kg Impactor at 10 m/s and 14% for the 6.3 kg impactor at 12 m/s. Also the slow increase in acceleration after the initial peak is in the same order of magnitude, but with some oscillations not seen in the experiment.

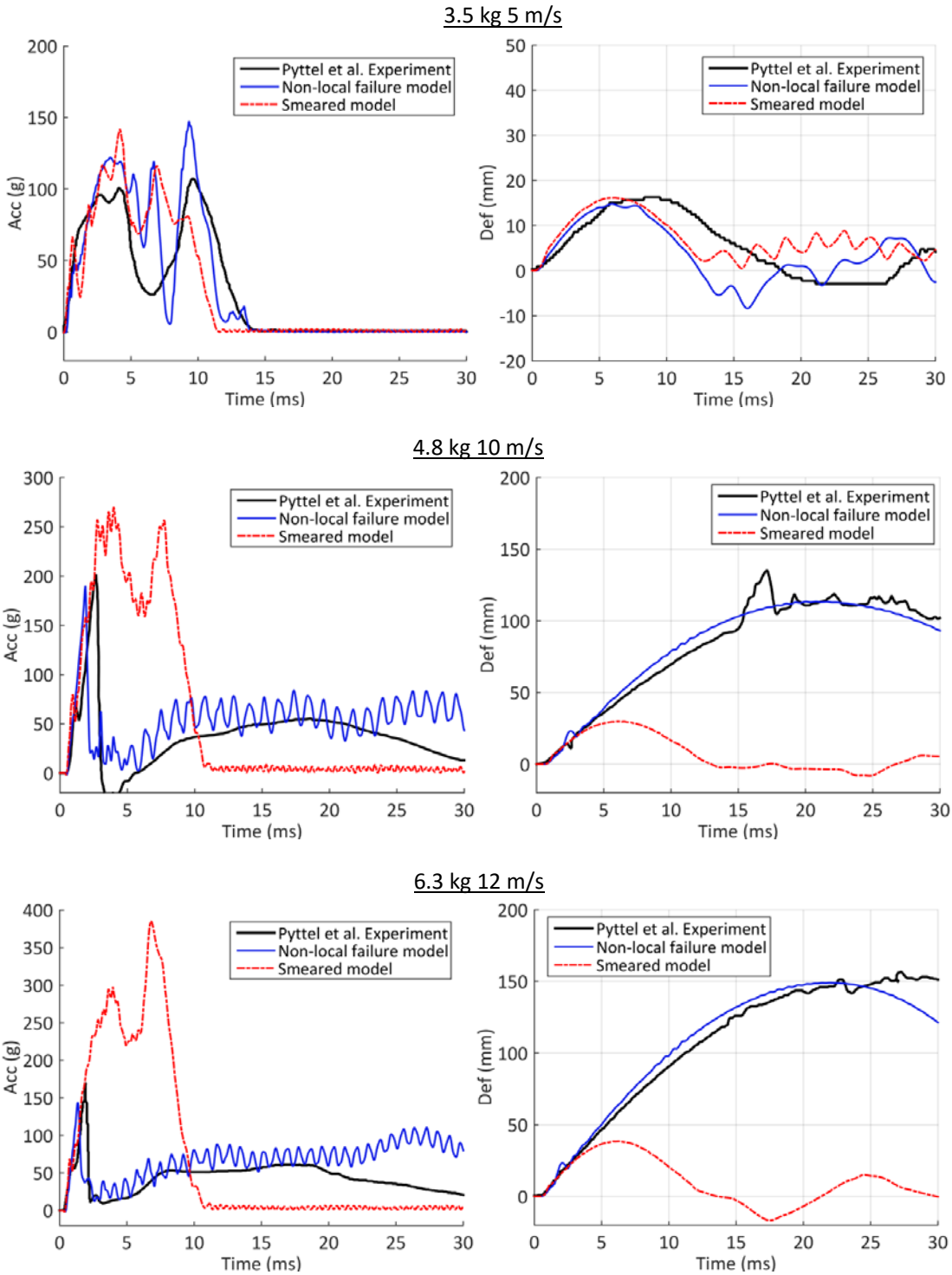

Fig. 2. Acceleration from head impactor (*left column*) and deformations at the centre of plate (*right column*) presented from top to bottom row for 3.5 kg 5 m/s, 4.8 kg 10 m/s and 6.3 kg 12 m/s, respectively. The experiment from [16] is drawn in solid black, the two models used in the current study are presented in solid blue and dashed red.

In Fig. 12 to Fig. 14 in Appendix E the deformation of the plate at the sensor positions is plotted as a function of the radius, and is presented for times t = 2, 5, 10 and 20 ms. The experimental results in [16] are compared with the non-local failure model and smeared model. For the 3.5 kg impactor (Fig. 12), the results agree well with both models, but the deformation is also quite limited. For both the 4.8 kg impactor (Fig. 13) and the 6.3 kg impactor (Fig. 14) using the non-local failure model, the deformation agrees well with the experiment up to 20 ms, with a max difference in displacement of a few millimetres. After 20 ms the deviation is slightly larger with a maximum difference of 10 mm, but only at more than 100 mm from the centre. The smeared model only agrees relatively well up to 5 ms and thereafter grossly under-predicts the deformation.

Windscreen Impact

In Fig. 3 the accelerations from the 4.8 kg impactor are shown from the impact against a windscreen at 10m/s from both outside (*left plot*) and inside impact (*right plot*). The non-local failure model exhibits a similar behaviour as the experiments, where the initial peak has a similar timing and duration, as well as a secondary smaller increase over a long duration. When impacting from the outside, the acceleration at the first peak is under-predicted by about 18%, and when impacting form the inside it is over-predicted by 70%. For the smeared model, the first peak for the outside impact is in the same range as the non-local failure model, but it also shows an even larger second peak not seen in the experiments at about 11 ms (*left plot*, Fig. 3). For the inside impact the acceleration peak is about three times as wide in duration and over-predicted by about 300%.

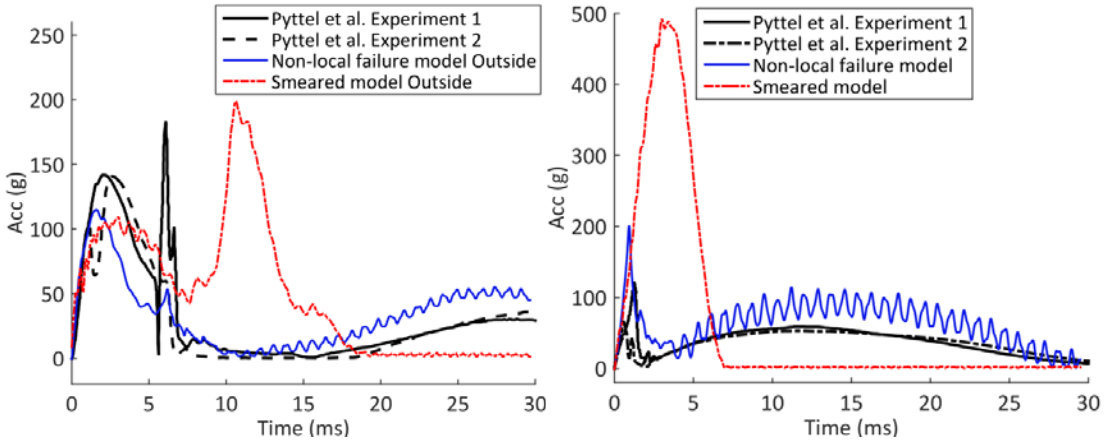

Fig. 3. Accelerations from NCAP impactor at 4.8 kg and 10 m/s impacting from outside of windscreen (*left*) and inside of windscreen (*right*).

Head Model Simulation

In Fig. 4 and Fig. 5 the maximum principal strain of all elements in the brain is plotted as a function of time for the four head orientations (centre front and centre side; edge front and edge side) and the two velocities (40 km/h and 60 km/h), comparing the results using the non-local failure model and the smeared model. It can be observed that there is a fairly good agreement between the two windscreen models in the two centre impacts at 40 km/h (Fig. 4, centre front and centre side). The two models give the same curve shape and a maximum difference of 5% in strain up to 10 ms. A second and equally large peak is, however, only observed for the non-local failure model. In general, the agreement between models is poor, with a difference between 8% and 40%, but especially in the shape of the strain-time curve. For the smeared model an initial high peak is consistently seen, followed by a decrease in strain. For the non-local failure model, on the other hand, the peak occurs later in the simulations, if not as for the two aforementioned impacts, with two peaks. In the edge side impacts, seen in the two bottom rows of Fig. 5, there is also a sudden increase in strain when using the non-local failure model not seen when using the smeared model. For each model in Fig. 4 and Fig. 5, the strain in a section plane of the brain is also shown for two time points corresponding to a peak strain value in either (or both) of the two simulations. For each impact condition and time point, the same section plane is used for both models; a sagittal plane for the front impacts and a coronal plane for the side impacts. These images show that the location of the highest strains is similar for the two models in the centre impacts, but with different timing. In the edge impacts, however, the location of the strain is changed to a much larger extent.

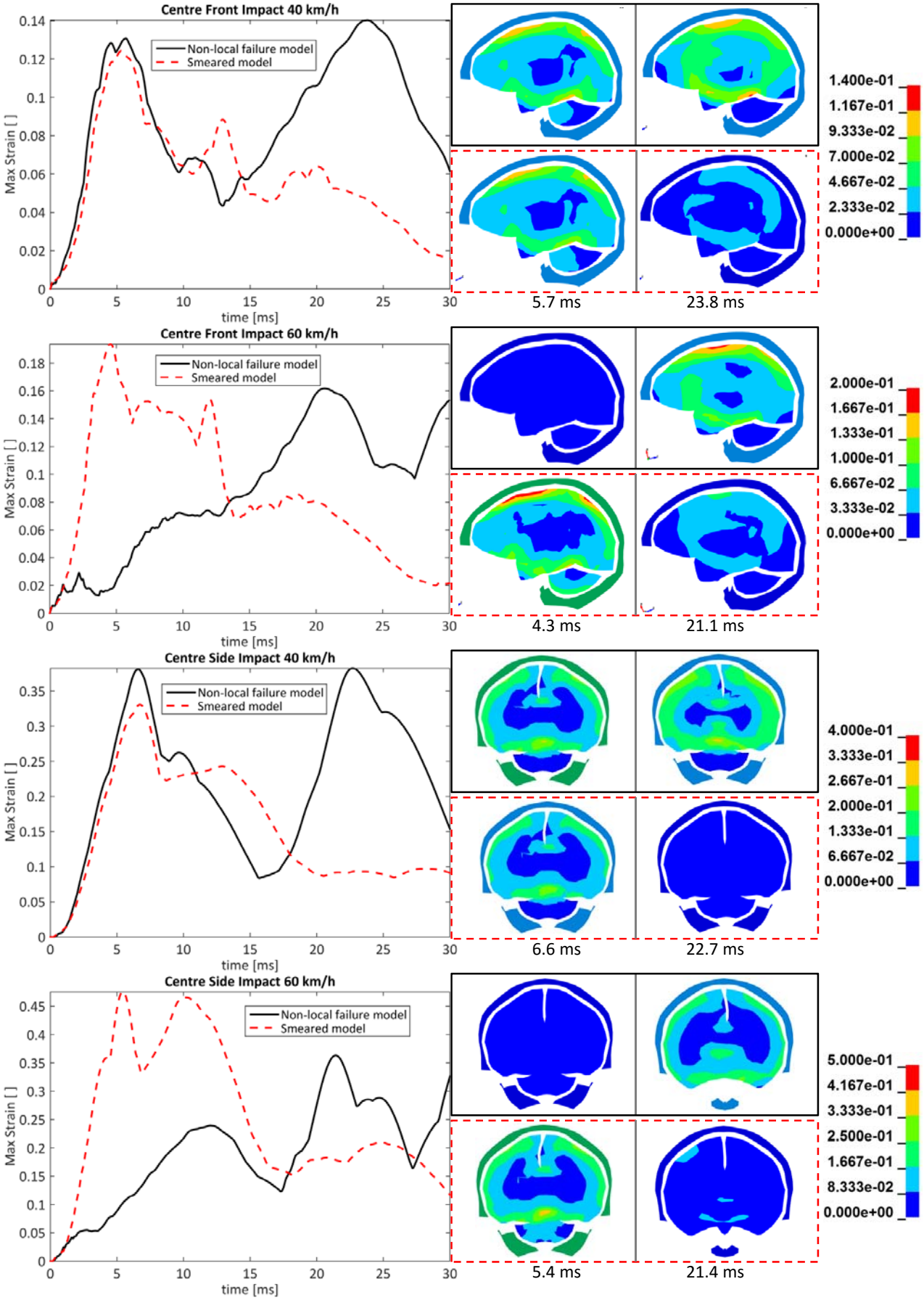

Fig. 4. Maximum strain in the brain, from top to bottom, impact at: center front 40 km/h, center front, 60 km/h, center side 40 km/h, center side 60 km/h, comparing the non-local failure and smeared model.

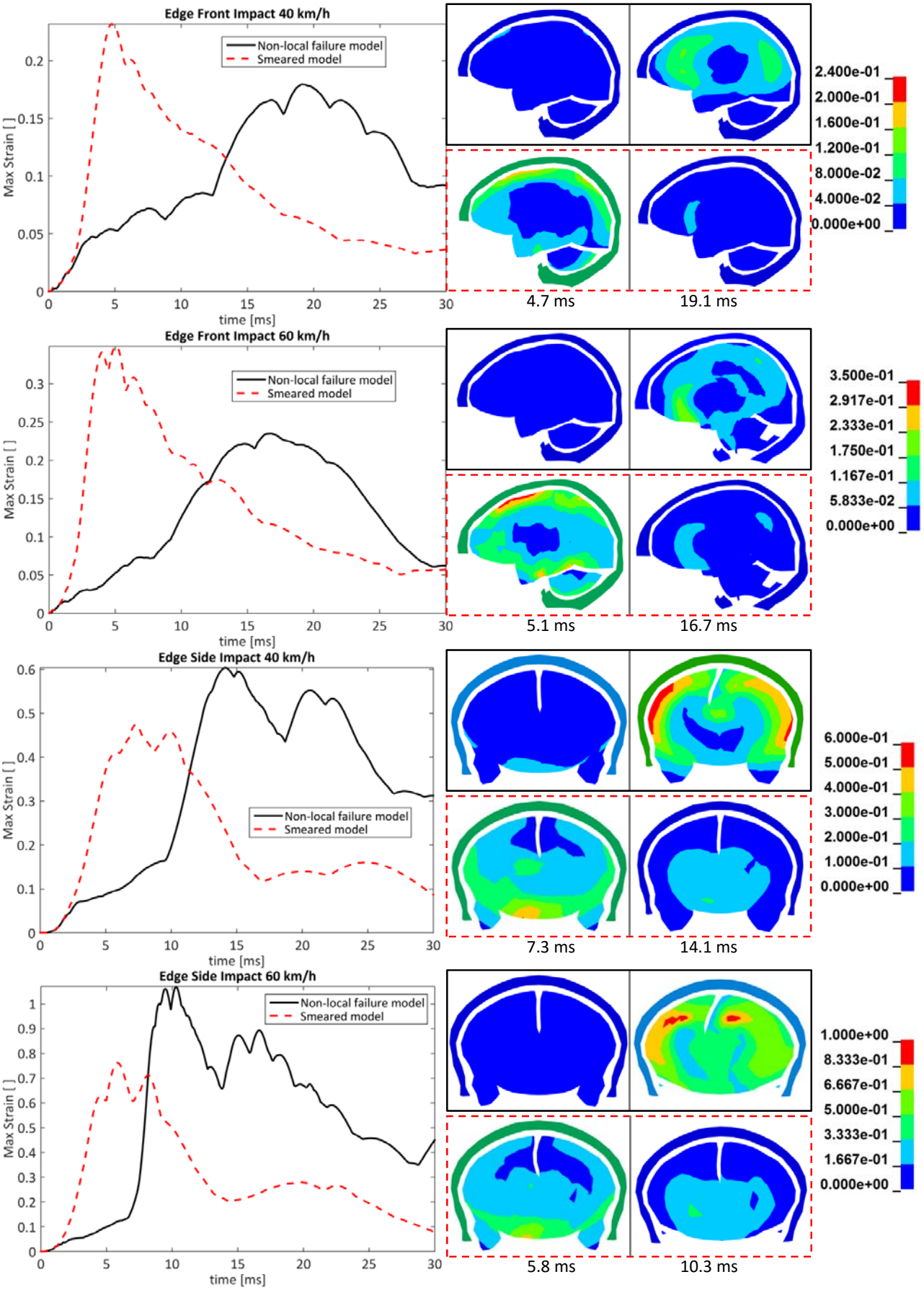

Fig. 5. Maximum strain in the brain, from top to bottom, impact at: edge front 40 km/h, edge front, 60 km/h, edge side 40 km/h, edge side 60 km/h, comparing the non-local failure and smeared model.

IV. DISCUSSION

This study implements two approaches of modelling vehicle windscreens, comparing their deformation and acceleration predictability, as well as assessing the effect of the two approaches on brain injury prediction.

The results of the comparison with a circular plate impact show that if the glass layers do not fail, the response in terms of both deformation and acceleration can be captured by either of the two modelling approaches used in this study. On the other hand, when the glass fails, only the non-local failure model shows capability of capturing both accelerations and deformations to an acceptable degree (Fig. 2). The smeared model, however, fails to capture the acceleration peak and the duration, as well as the degree of deformation, with an error not considered acceptable. One explanation for this could be the assumption that one side of the glass is maintained intact in the smeared model. Although this is likely a sound assumption for smaller deformations of pure bending, the effective Young's modulus after failure of E^{II} = 16.5 GPa is probably much too high a value, being more than six times larger than that of the Young's modulus for PVB. In the non-local failure model, the load-carrying capacity after glass failure is almost solely due to the PVB since the glass breaks on both sides relatively simultaneously and the elements are deleted to such an extent that it would not be able to carry much, if any, load. This also indicates that for the non-local failure approach introduced in [16], the increase in acceleration is mostly due to the stiffness of the glass (being more than 28 times that of PBV). Further, the time of drop in acceleration also occurs at the expected time, being the moment of failure of the glass, due to the developed failure criterion. After failure, an oscillating acceleration response can be seen for the non-local failure model (Fig. 2), which is most likely a side effect of the element deletion in the glass layer. These oscillations can be observed visually in the outer rubber surface of the impactor due to the sudden loss of load-carrying material directly in contact with the impactor. However, this effect is assumed to have a minor influence on the injury predictability of head impacts, and is left for further investigation.

The non-local failure model also seems capable of capturing the deformation of the circular plate as a function of the radius relatively well, also for points further away from the centre (Fig. 12 to Fig. 14 in Appendix E). Deviations from the experimental results are mainly seen at 20 ms and at a distance larger than 5 cm from the centre; see Fig. 13 and Fig. 14. This could possibly be due to different change in mass of the windscreen when the glass fails. When the impactor hits the plate in the experiments, some of the glass is most likely to be removed, but the removed mass is likely to be higher in the simulations than in the experiments due to the element deletion, since the mesh size is relatively large. This is, however, not considered a large drawback for injury prediction since the deformation close to the head is assumed to be of most importance.

The results from the outside impacts to the full windscreen show that the initial acceleration peak is captured to a similar degree of accuracy with both models. After failure, however, the smeared model shows a second, larger peak (left plot in Fig. 3) not seen in the experiment. This is most likely due to the relatively high stiffness, causing the windscreen to act as a springboard, only delaying the spring-back due to the geometry of the windscreen. For the non-local failure model, the fracture seems to occur at the expected time and the shape of the acceleration-time plot follows the experiment fairly well, though the same oscillations described above can be observed here as well. For the impact from the inside to the full windscreen, both models over-predict the acceleration peak, although using the smeared model it is over-predicted by about 300% with a duration about three times as long as the experiment. The non-local failure model has similar peak duration as the experiment and overall shape of the curve, but still over-predicting by about 100%. The differences seen in the initial peak levels could be due to differences in windscreen geometry, specifically the radius of curvature, although they are unknown as the geometry of the windscreen of the experiments were not published and an available windscreen was used instead. The differences are however only large for the inside impact which is not as relevant for pedestrian impacts as the outside impact.

One limitation with the evaluation of the models is the relatively small sample of experiments used. This could be further improved if more experiments are made available, but it should also be noted that the experiments used were well controlled and therefore suitable for this type of evaluation. A limitation with the study on brain injury was the lack of a body connected to the head model. This was a simplification made in order to facilitate the parametric study and to reduce the calculation time. Although the body can probably have some influence in the later stage of the impact, it is not considered a major drawback as the study only compared the different initial conditions and has as its primary goal the comparison of the two windscreen models. This does, however, put some limitations on conclusions regarding specific injury levels, which may be

different with a body connected.

The effect of the windscreen modelling approach on head injury prediction is seen in the results from the FE head simulations in Fig. 4 and Fig. 5. It reveals that the effect on tissue strain is not only on the peak value but especially on the shape of the strain-time curve. In two cases, however, the first peak agrees fairly well between the two models (centre front and centre side impacts at 40 km/h in Fig. 4), although a secondary peak can be observed for the non-local failure model not seen for the smeared model. The explanation for the absence of this secondary peak using the smeared model is that with this model, the head is only in contact until about 15 ms, after which the head recoils away from the windscreen. With the non-local failure model, the head continues to collide in the same direction into the windscreen. In all the other impact cases using the non-local failure model, the initial peak is almost completely absent and only the peak values are comparable using the two windscreen models. The explanation for this is the fact that in all but the two aforementioned impacts, the glass layers in the non-local failure model fracture very early in the simulation, after about 0.5 to 1 ms from head contact instead of about 5 ms. In the case of a late windscreen fracture, the highly stiff windscreen deforms as a whole as the motion of the head is changed. The strain increase and peak also correlate well with the duration of intact windscreen deformation and the time of fracture. In the case of an early fracture, the windscreen deforms more locally and mostly in the much softer PVB, which is why a high peak strain value is instead obtained when the head motion is changed by the PVB as it is stretched out and stiffens. The stretching of the PVB also correlates well with the secondary peak seen in the two late fracture impacts. This effect is not seen with the smeared model, as the glass always fractures shortly after contact and the remaining layer is much stiffer than the PVB. For the higher speed impacts, the earlier failure of the glass is also consistent with the experimental results from Pyttel *et al.* [16], where a lower acceleration is seen for the heavier impactor at a higher impact speed (see Fig. 2). The absence of an initial peak and early glass fracture can also be observed for the lower 40 km/h edge impacts using the non-local failure model. This is probably due to the very stiff boundary condition of the frame, being rigidly constrained, leading to a higher strain on the glass. It can also be observed that the peak strain for these impacts occurs earlier in time as a consequence of being closer to the frame where the PVB cannot deform to the same extent. For the edge-side impacts, the sharp increase in strain observed with non-local failure model (see last two rows in Fig. 5) is most likely an effect of the head coming into contact with the frame, causing a sudden rotation, due to the fact that the head covers a larger area in this orientation. These effects are not seen with the smeared model as the deformation of the windscreen is never large enough for the head to come in contact with the frame and the effect of the constrained boundary condition on the intact layer is most likely smaller. This effect would also explain the large difference in location of strain between the two models for the edge impacts seen in the in section plane images in Fig. 5, compared to the centre impacts in Fig. 4.

V. CONCLUSIONS

This study shows that a non-local failure model can capture both accelerations and deformations of a head-like impact to a windscreen, with a maximum error of about 18% in acceleration and even less in deformation. This level of agreement is not possible with a smeared modelling technique, showing errors in the range of 40% to 300%, expect for cases where the windscreen does not fracture. Further it can be concluded that the large deformations and time of fracture predicted with the non-local failure model, but not the smeared model, has a large effect on the timing, level and location of strains experienced in the brain during a windscreen impact. It is also shown that these properties are especially important in impacts close to the A-pillar.

VI. ACKNOWLEDGEMENT

This work has been carried out in association with SAFER - Vehicle and Traffic Safety Centre at Chalmers, Sweden. Partners from SAFER active in this project are Autoliv and Volvo Cars. The authors acknowledge FFI (Strategic Vehicle Research and Innovation), Sweden, for part-financing the project.

VII. REFERENCES

[1] Naci, H., Chisholm, D., Baker, T. D. (2009) Distribution of road traffic deaths by road user group: a global comparison. *Inj. Prev.*, **15**(1): pp.55–59.

[2] Otte, D. Severity and mechanism of head impacts in car to pedestrian accidents. *Proceedings of The IRCOBI conference*, 1999, Sitges, Spain pp.329–341.

[3] Mizuno, K., Kajzer, J. Head Injuries in Vehicle-Pedestrian Impact. *Proceedings of SAE World Congress & Exhibition*, 2000, Detroit, USA.

[4] Fredriksson, R., Rosén, E., Kullgren, A. (2010) Priorities of pedestrian protection - A real-life study of severe injuries and car sources. *Accid. Anal. Prev.*, **42**(6): pp.1672–1681.

[5] Holbourne, A. H. (1943) Mechanics of head injuries. *Lancet*, **242**: pp.438–441.

[6] Hirsch, A. E., Ommaya, A. K. Protection from Brain Injury - The Relative Significance of Translational and Rotational Motions of the Head after Impact. *Proceedings of 14th Stapp Conference*, 1970, Michigan, USA pp.144–151.

[7] Gennarelli, T. A., Thibault, L. E., Ommaya, A. K. Pathophysiologic Responses to Rotational and Translational Accelerations of the Head. *Proceedings of 16th Stapp Car Crash Conference*, 1972, Detroit, USA pp.296–308.

[8] Larcher, M., Solomos, G., et al. (2012) Experimental and numerical investigations of laminated glass subjected to blast loading. *Int. J. Impact Eng.*, **39**(1): pp.42–50.

[9] Wei, J., Dharani, L. R. (2006) Response of laminated architectural glazing subjected to blast loading. *Int. J. Impact Eng.*, **32**(12): pp.2032–2047.

[10] Zhang, X., Hao, H., Ma, G. (2013) Parametric study of laminated glass window response to blast loads. *Eng. Struct.*, **56**: pp.1707–1717.

[11] Bennison, S., Jagota, A., Smith, C. (1999) Fracture of glass/poly (vinyl butyral)(Butacite®) laminates in biaxial flexure. *J. Am. Ceram. Soc.*, **82**(7): pp.1761–1770.

[12] Thompson, G. M., Kilgur, A. Detailed Windscreen Model for Pedestrian Head Impact. *Proceedings of 9th LS-DYNA Forum*, 2010, Bamberg, Germany pp.1–30.

[13] Sun, D., Andrieux, F. Modelling of the failure behaviour of windscreens and component tests. *Proceedings of LS-DYNA Anwenderforum*, 2005, Bamberg, Germany pp.23–32.

[14] Timmel, M., Kolling, S., et al. (2007) A finite element model for impact simulation with laminated glass. *Int. J. Impact Eng.*, **34**(8): pp.1465–1478.

[15] Peng, Y., Yang, J., et al. (2013) Finite element modeling of crash test behavior for windshield laminated glass. *Int. J. Impact Eng.*, **57**: pp.27–35.

[16] Pyttel, T., Liebertz, H., Cai, J. (2011) Failure criterion for laminated glass under impact loading and its application in finite element simulation. *Int. J. Impact Eng.*, **38**(4): pp.252–263.

[17] Galuppi, L., Royer-Carfagni, G. (2012) Laminated beams with viscoelastic interlayer. *Int. J. Solids Struct.*, **49**(18): pp.2637–2645.

[18] Ing, P., Froli, M., Lani, I. L. Adhesion , creep and relaxation properties of PVB in laminated safety glass. *Proceedings of Glass Perfomance Days*, 2011, pp.1–4.

[19] Du Bois, P. a., Kolling, S., Fassnacht, W. (2003) Modelling of safety glass for crash simulation. *Comput. Mater. Sci.*, **28**(3)–(4 SPEC. ISS.): pp.675–683.

[20] Xu, J., Li, Y., et al. (2011) Experimental investigation on constitutive behavior of PVB under impact loading. *Int. J. Impact Eng.*, **38**(2)–(3): pp.106–114.

[21] Flocker, F. W., Dharani, L. R. (1997) Stresses in laminated glass subject to low velocity impact. *Eng. Struct.*, **19**(10): pp.851–856.

[22] LSTC. LS-DYNA KEYWORD USERS'S MANUAL. *Livermore Software Technology Corporation*, Livermore, California: 2002.

[23] Hooper, P. a., Blackman, B. R. K., Dear, J. P. (2011) The mechanical behaviour of poly(vinyl butyral) at different strain magnitudes and strain rates. *J. Mater. Sci.*, **47**(8): pp.3564–3576.

[24] Juntikka, R., Kleiven, S., Hallström, S. (2004) Optimization of single skin surfaces for head injury prevention–a comparison of optima calculated for global versus local injury thresholds. *Int. J. Crashworthiness*, **9**(4): pp.365–379.

[25] Kleiven, S. (2007) Predictors for traumatic brain injuries evaluated through accident reconstructions. *Stapp Car Crash J.*, **51**: pp.81–114.

[26] Kleiven, S., Hardy, W. N. (2002) Correlation of an FE Model of the Human Head with Local Brain Motion--Consequences for Injury Prediction. *Stapp Car Crash J.*, **46**: pp.123–144.

[27] Kleiven, S. (2006) Evaluation of head injury criteria using an FE model validated against experiments on localized brain motion, intra-cerebral acceleratio, and intra-cranial pressure. *Int. J. Crashworthiness*, **11**(1): pp.65–79.

[28] Gennarelli, T. A., Thibault, L. E., et al. (1982) Diffuse Axonal Injury and Traumatic Coma in the Primate. *Ann. Neurol.*, **12**(6): pp.564–574.

[29] Galbraith, J. a, Thibault, L. E., Matteson, D. R. (1993) Mechanical and electrical responses of the squid giant axon to simple elongation. *J. Biomech. Eng.*, **115**(1): pp.13–22.

[30] Bain, A. C., Meaney, D. F. (2000) Tissue-Level Thresholds for Axonal Damage in an Nervous System White Matter Injury. *J. Biomech. Eng.*, **122**(6): pp.615–622.

[31] Morrison, B., Cater, H. L., et al. (2003) A tissue level tolerance criterion for living brain developed with an in vitro model of traumatic mechanical loading. *Stapp Car Crash J.*, **47**: pp.93–105.

[32] Shreiber, D., Bain, A., Meaney, D. In vivo thresholds for mechanical injury to the blood-brain barrier. *Proceedings of the 41 Stapp Car Crash Conference*, 1997, Warrendale, USA.

VIII. APPENDIX

Appendix A: Mesh Convergence Flat Plate Impact

In Fig. 6 the accelerations and deformations from the flat plate impact are shown from simulation with four different mesh densities using the non-local failure model.

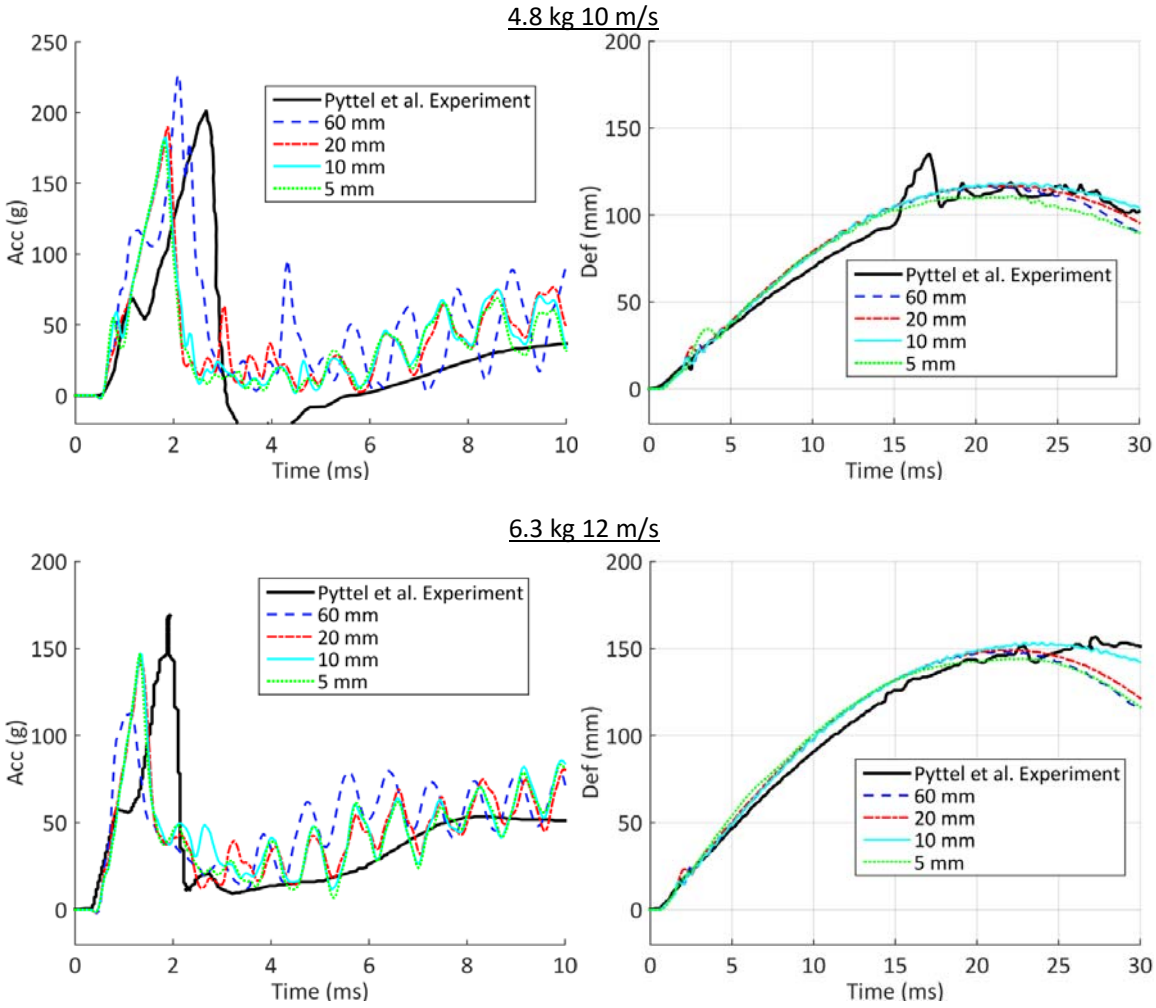

Fig. 6. Resultant acceleration from head impactor (*left column*) and deformations at the centre of plate (*right column*) presented from top to bottom row for, 4.8 kg 10 m/s and 6.3 kg 12 m/s, respectively. The experiment from [16] is drawn in solid black.

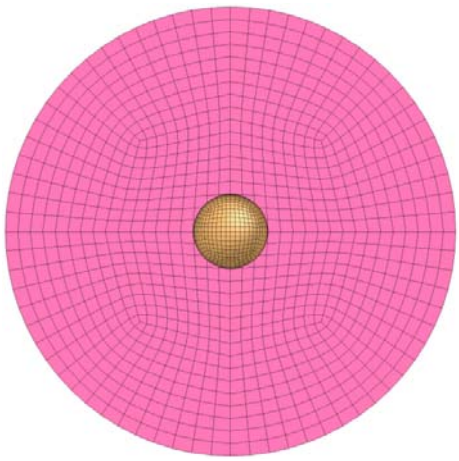

Fig. 7. 20 mm mesh of flat plate used in NCAP impact simulations.

Appendix B: Material Properties for Windscreen Models

TABLE II
MATERIAL PROPERTIES OF GLASS AND PVB FROM [15] AND CALCULATED SMEARED PARAMETERS

Property	Glass	PVB	Smeared parameters	
ρ	2500 kg/m^3	1100 kg/m^3	t_E	3.5 mm
E	74 GPa	2.6 GPa	ρ_E	1426.9 kg/m^3
v	0.227	0.435	E^{II}	16.5 GPa
σ_y	50 Mpa	--	$E_{G,mod}$	131.6 GPa
ϵ_{fail}	0.001	--	--	--

TABLE III
MATERIAL PROPERTIES FROM [16] USED IN THE NON-LOCAL FAILURE MODEL

Property	Glass	PVB
ρ	2500 kg/m^3	1100 kg/m^3
E	70 GPa	--
v	0.25	0.495
σ_y	60 Mpa	--
E_c	22.3 kNmm	--
R_c	210 mm	--

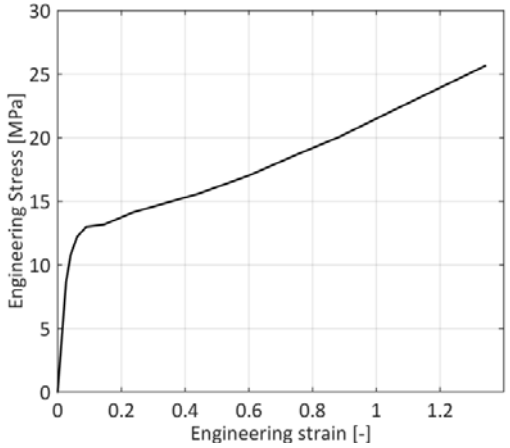

Fig. 8. Stress strain relationship for PVB at strain rate 60 s^{-1} [23] used in the non-local failure model.

Appendix C – Dimensions of Windscreen, Head Relative Position and Impact Angle

Fig. 9 shows the dimensions of the windscreen model used in the head impact simulations and the relative position of the head measured from the centre of gravity (CG) for both centre and edge impacts. The relative positions are the same for both front and side impact. Fig. 10 shows the head initial velocity given in the direction of the Frankfurt plane with an angle relative a line connecting the corners of the windscreen. The same direction and angle is used in all head impact simulations.

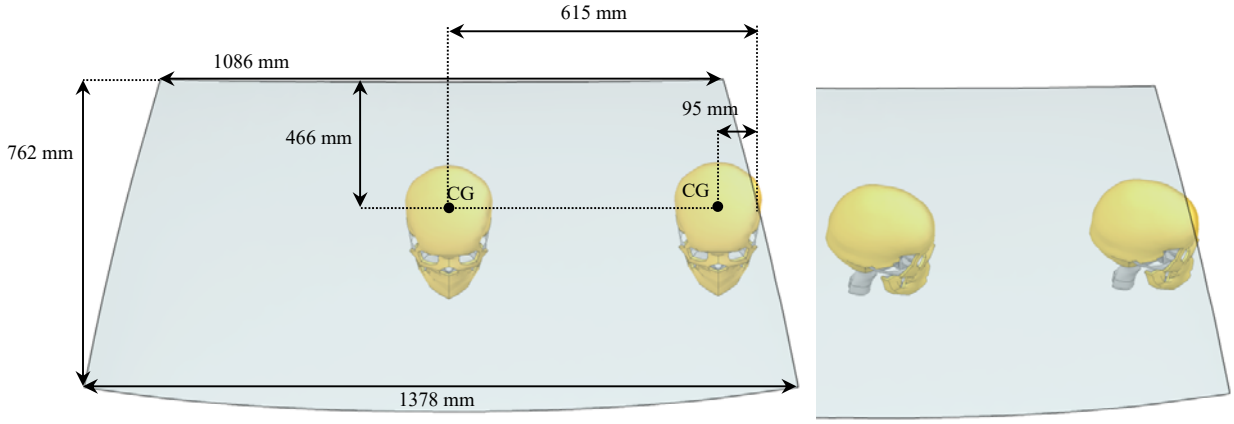

Fig. 9. KTH head model positioned in relation to windscreen (*seen from the inside*) with dimensions. Left figure shows the head with the face towards the windscreen for both centre and edge impacts. The right figure shows the head positioned with a 90 degree rotation, for both centre and edge impacts.

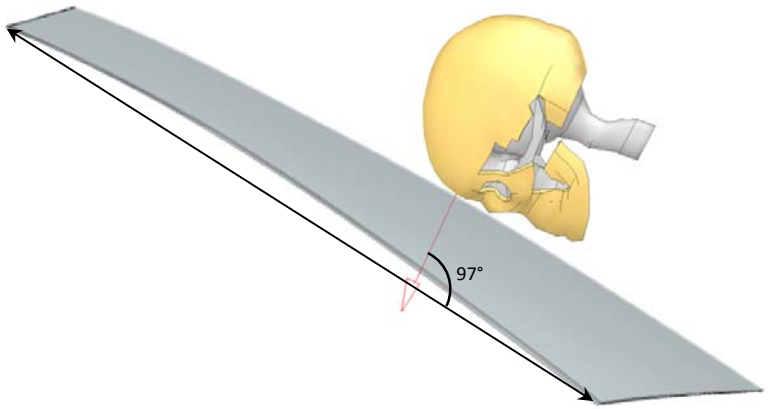

Fig. 10. Impact velocity vector for the head and the angle relative the windscreen used in all head impact simulations.

Appendix D - The KTH FE Head Model

The head model includes the scalp, the skull, the brain, the meninges, the cerebrospinal fluid (CSF) and eleven pairs of the largest parasagittal bridging veins, see Fig. 11, with material properties adapted from the study by [25] listed in TABLE IV. To accommodate large elastic deformations of the brain, a second order Ogden hyperelastic constitutive model was used together with a linear viscoelastic model. The constitutive constants used for the brain tissue are also adapted from [25] and presented in TABLE V.

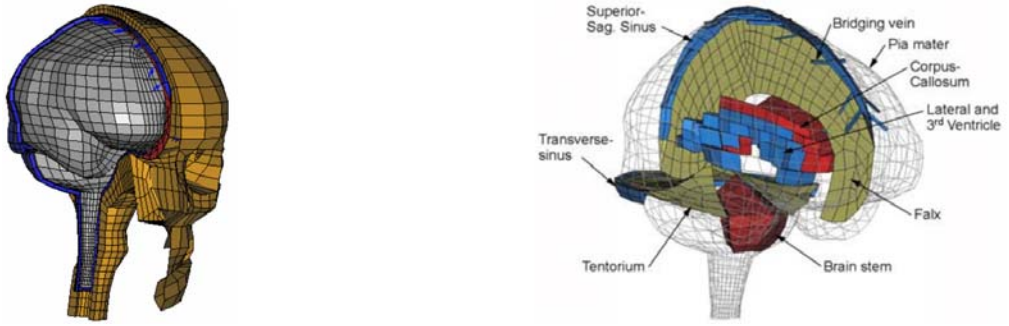

Fig. 11. Finite element model of the human head.

TABLE IV
MATERIAL PROPERTIES USED FOR THE FE HEAD MODEL

Tissue	*Young's modulus* [MPa]	*Density* [kg/dm^3]	Poisson's ratio
Outer compact bone	15 000	2.00	0.22
Inner compact bone	15 000	2.00	0.22
Porous bone	1000	1.30	0.24
Brain	Hyper-Viscoelastic	1.04	0.49999
Cerebrospinal Fluid	*K* = 2.1 GPa	1.00	-
Sinuses	*K* = 2.1 GPa	1.00	-
Dura mater	31.5	1.13	0.45
Falx/Tentorium	31.5	1.13	0.45
Pia mater	11.5	1.13	0.45
Scalp	Hyper-Viscoelastic	1.13	0.42
Bridging veins	EA = 1.9 N		

K = Bulk modulus, and EA = Force/unit strain.

TABLE V
OGDEN HYPERELASTIC AND LINEAR VISCOELASTIC CONSTANTS

Parameter	Value
μ_1 (Pa)	53.8
μ_2 (Pa)	-120.4
α_1	10.1
α_2	-12.9
G_1 *(MPa)*	0.32
G_2 *(kPa)*	78
G_3 *(kPa)*	6.2
G_4 *(kPa)*	8.0
G_5 *(kPa)*	1.0
G_6 *(kPa)*	3.0
β_1 (1/s)	10^6
β_2 (1/s)	10^5
.	.
.	.
β_6 (1/s)	10^1

Appendix E – Sensor displacement for Flat Plate NCAP Impact

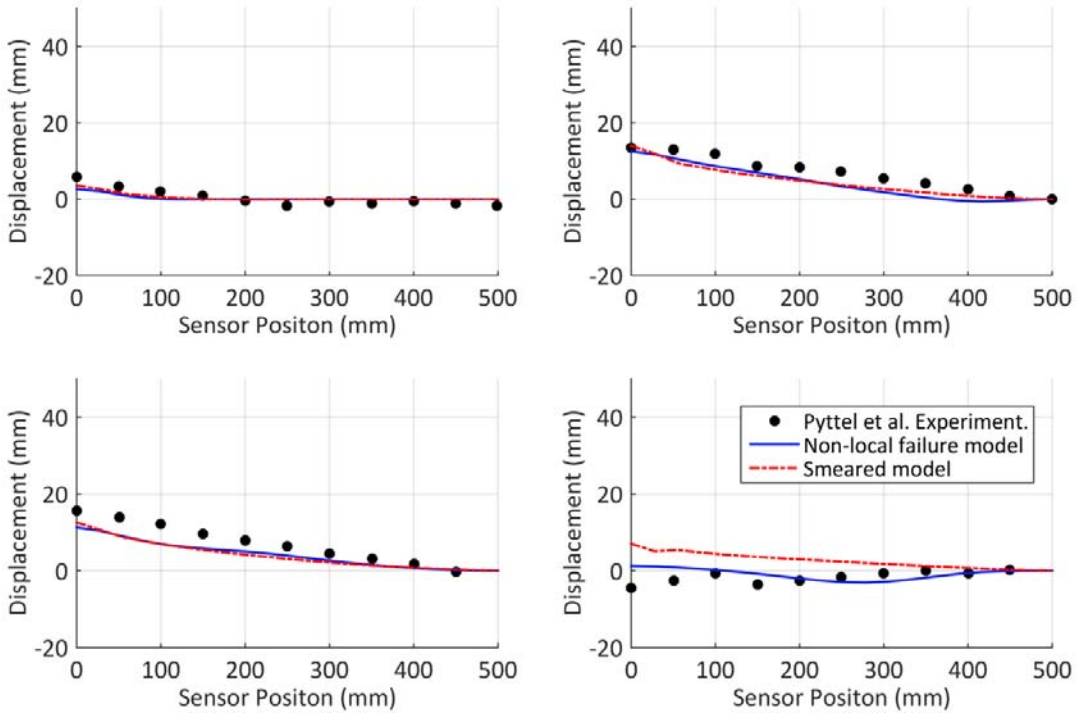

Fig. 12. Displacement of sensor positions marked with dots as function of radius of plate, using NCAP head of 3.5 kg at 5 m/s, at time t=2 ms (*upper left*), t=5 ms (*upper right*), t=10 ms (*lower left*) and t=20 ms (*lower right*).

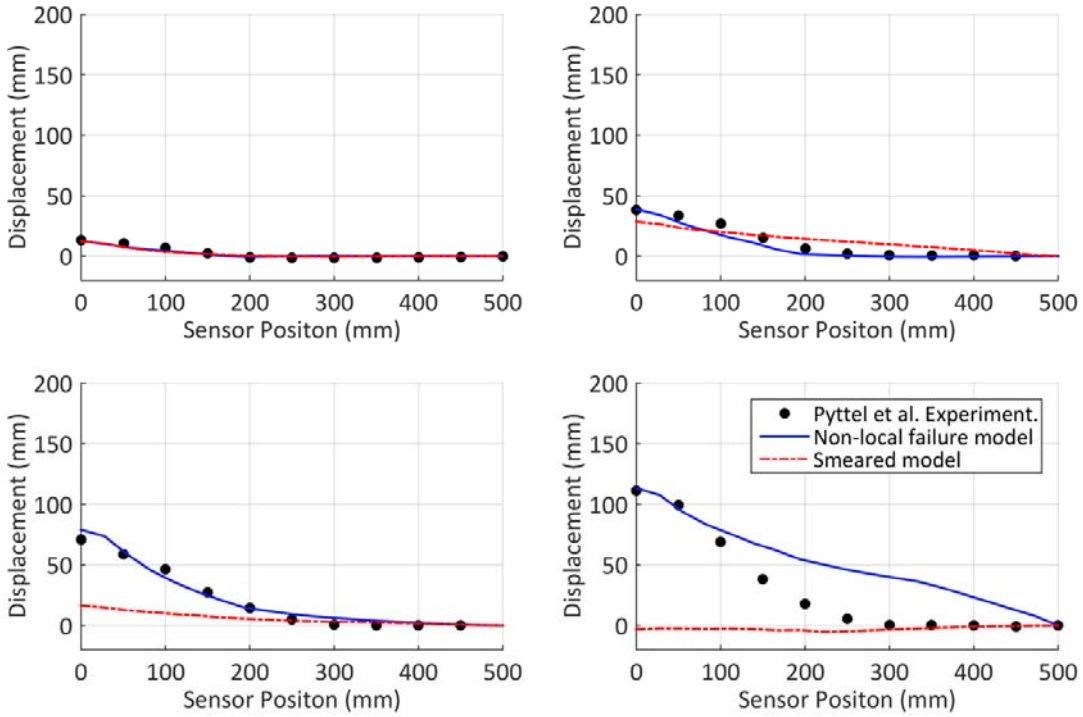

Fig. 13. Displacement of sensor positions marked with dots as function of radius of plate, using NCAP head of 4.8 kg and 10 m/s, at time t=2 ms (*upper left*), t=5 ms (*upper right*), t=10 ms (*lower left*) and t=20 ms (*lower right*).

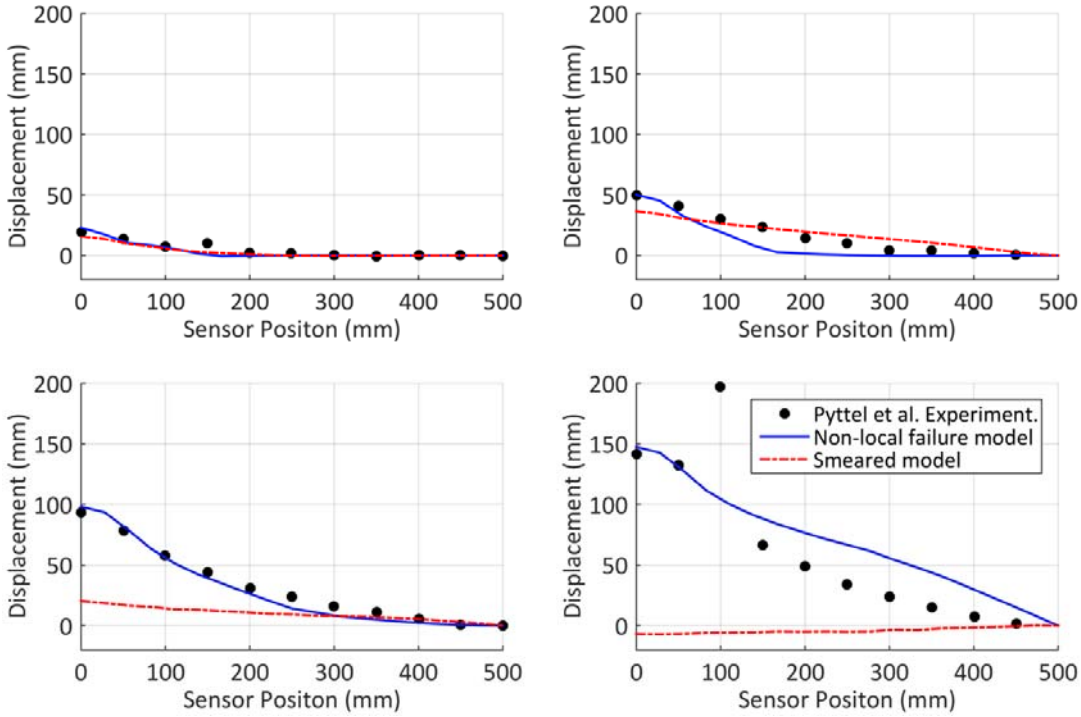

Fig. 14. Displacement of sensor positions marked with dots as function of radius of plate, using NCAP head of 6.3 kg and 12 m/s, at time t=2 ms (*upper left*), t=5 ms (*upper right*), t=10 ms (*lower left*) and t=20 ms (*lower right*[*]).

**The experimental data comes directly from* [16] *and though the third point from the centre deviates in this plot no explanation is given in the paper.*